

## Probing quark gluon plasma with jets

Jicai Pan and Charles Gale

*Department of Physics, McGill University  
3600 University St., Montréal, PQ, H3A 2T8 Canada*

### Abstract

We study multiple scatterings of jets on constituents of quark gluon plasma and introduce energy–energy correlations to quantify their effects. The effects from a longitudinally expanding plasma on medium as well as high energy jets are found to be significant at both RHIC and LHC energies. Because jets escape from the plasma long before the completion of mixed phase, these effects are free from complications of final state hadronic interactions and decays. These suggest that jets can be used to probe the plasma that might be created in future high energy heavy ion collisions.

PACS numbers: 25.75.+r, 12.38.Mh, 24.85.+p, 12.38.Bx

# 1 Introduction

In high energy nuclear collisions new states of matters, e.g. the quark gluon plasma predicted by numerical calculations of lattice gauge theories, might be produced. Because of the many-body heavy-ion system and soft multi-hadronic production, major efforts are to find experimental observables that could provide information on the states of matters produced in the collisions [1]. Many observables that have been intensively studied are mostly products created in the plasma, like dileptons, photons,  $J/\psi$  and strange particles. These processes can carry information about the plasma, but some of them are usually complicated by final state hadronic interactions and decays.

In this paper we are interested in jets propagating through the plasma. It is of great interest for following reasons. (a) Jets have been extensively investigated both experimentally and theoretically. Because they are produced by hard collisions of quarks and gluons, they can be and have been calculated with perturbative QCD to various degrees of accuracy. The agreement between theory and experiments shows that jets are one of the very few well understood high energy strong interacting phenomena. (b) Jets are produced at the very beginning of the collision process and they propagate in the plasma and interact strongly with the plasma constituents before they escape. Because of these properties they can be used to probe the plasma. (c) Since the final state hadronic interactions and decays take place after the phase transition that is expected to complete after the jets escape from the plasma, the jet signals are virtually free of background of final state interactions and decays. (d) Jets are easily accessible experimentally. The typical jet energy is greater than 10 GeV which is much larger than the typical energies of constituents in a thermalized plasma at the temperature that can be created in the future heavy ion collider, such as the RHIC and the LHC. Jets are therefore expected to escape from the plasma as well identified objects.

The energy–energy correlations of hadrons produced in  $e^+e^-$  collider were suggested by Basham, Brown, Ellis and Love [2] to test QCD, and were investigated by a number of experimental groups [3]. In hadronic and nuclear collisions jets are produced by hard scattering of partons. In a  $2 \rightarrow 2$  process the two jets are produced back-to-back in their rest frame. Thus the QCD contribution to the energy–energy correlations is dominated by  $2 \rightarrow 3$  process. Ali, Pietarinen and Stirling [4] showed that transverse energy–energy correlations depend very weakly on the structure function and the normal-

ized correlation function is approximately proportional to coupling constant  $\alpha_s$ .

A jet produced at the beginning of a collision may scatter many times on plasma constituents before it escapes from the plasma. The average transverse momentum gained in the multiple scattering can be as high as a few GeV. This effect on a jet of energy of several tens GeV is of the order of  $\alpha_s$ . In fact, as we shall see the multiple scattering has significant effects on energy correlations and dominates over the QCD contribution in some cases.

The paper is organized as follows. In section 2 we start with definition of energy–energy correlation and derive a general formalism for evaluating the scattering effects on correlations. We then calculate these effects in a longitudinal hydrodynamical model that describes plasma expansion. Hadronization effects are discussed at the end of the section. In section 3 we present the numerical results and discuss their dependence on colliding energy, jet energy and nuclear size. In section 4 we summarize our conclusions.

## 2 Jets in quark gluon plasmas

In nuclear collisions at RHIC and LHC energies, jet productions are no longer rare events. High transverse energy jets stand high beyond the associated soft productions and can be readily identified experimentally. Low transverse energy jets are, on the other hand, burried under the large amount of soft processes. To reduce the soft background, one studies high transverse energy jets. To see the effects of plasma on high  $E_T$  jets, it is essential to find sensitive variables. In the following, transverse energy–energy correlations are introduced to study such effects. As we shall see that the plasma indeed has significant effects on the correlations.

### 2.1 Energy–energy correlations and effects of plasmas

As aforementioned, the energy–energy correlations were introduced in [2] to test the QCD in  $e^+e^-$  collisions, and transverse energy–energy correlations were suggested in [4] to measure  $\alpha_s$  in  $p\bar{p}$  collision. In nuclear collisions we can similarly define the transverse energy–energy correlations for high  $E_T$

jets as

$$\frac{1}{\Sigma} \frac{d\Sigma}{d\phi}(E_T) = \left\langle \frac{1}{\Delta\phi} \sum_{i,j}^n \frac{E_{Ti} E_{Tj}}{E_T^2} \right\rangle_{event} \quad (1)$$

Here  $E_{Ti}$  is the transverse energy of particle  $i$ ,  $\Sigma = \int_0^{2\pi} (d\Sigma/d\phi) d\phi$ , and  $\Delta\phi$  is the angle between the particle pair  $(i, j)$  on the transversal plane. The  $\langle \dots \rangle_{event}$  means average over many events. To obtain higher statistics one might integrate over a range of transverse energies. In this case one has

$$\frac{1}{\Sigma} \frac{d\Sigma}{d\phi}(\Delta E_T) = \int_{E_T^{min}}^{E_T^{max}} dE_T \frac{d^2\Sigma}{dE_T d\phi} / \int_{E_T^{min}}^{E_T^{max}} dE_T \frac{d\Sigma}{dE_T} \quad (2)$$

The numerical calculation of correlation function has been done in ref. [4] based on the perturbative calculations of hard  $2 \rightarrow 2$  and  $2 \rightarrow 3$  processes in QCD [5].

Now let us consider the effects of the plasma. Because two-jet production dominates over multiple-jet production we need only to consider the plasma effects on two-jet events. Let  $p_\mu$  and  $p'_\mu$  be the four momenta of a jet before and after the multiple scattering off plasma constituents. In high energy elastic scattering, the scattering cross section depends only on four-momentum transfer squared, or the transverse momentum because  $-(p_\mu + p'_\mu)^2 = 4p^2 \sin^2(\eta/2) \approx p_T^2$ . The  $p_T$  distribution of the jet decreases rapidly with increasing  $p_T$  and vanishes in the backward hemisphere ( $\eta > \pi/2$ ). We assume that  $f_F(p_T)$  is the  $p_T$  distribution of one jet which we define as the forward jet and  $f_B(p_T)$  is that of the other jet in backward, and they satisfy the following normalization condition

$$\int \frac{d^3\mathbf{p}}{E} f_F(p_T) = \int \frac{d^3\mathbf{p}}{E} f_B(p_T) = 1. \quad (3)$$

Here  $E = Q/2$  and  $Q$  is the total jet energy. We note

$$\int \frac{d^3\mathbf{p}}{E} f_F(p_T) = \frac{1}{E} \int_0^E d^2\mathbf{p}_T f_F(p_T) \int_0^{\sqrt{E^2 - p_T^2}} dp_z. \quad (4)$$

After integrating over  $p_z$  one can expand  $\sqrt{E^2 - p_T^2}$  as  $E(1 - p_T^2/2E^2 + \dots)$ . As we shall see later that the effects of the plasma on jets are of the order of  $\langle p_T \rangle / E$ , we can neglect  $\langle p_T^2 \rangle / E^2$  and higher terms. That is

$$\int d^2\mathbf{p}_T f_F(p_T) = \int d^2\mathbf{p}_T f_B(p_T) = 1. \quad (5)$$

Let  $d\sigma/d\Omega_0$  be the cross section for two-jet production in a nuclear collision, with  $\Omega_0$  being the usual solid angle. The double energy cross section after the scattering on plasma constituents can be written as

$$\frac{d^2\Sigma}{d\Omega_1 d\Omega_2} = \frac{1}{2} \int d\Omega_0 \frac{d\sigma}{d\Omega_0} \int \frac{p_1^2 dp_1}{E_1} \frac{p_2^2 dp_2}{E_2} [f(\mathbf{p}_1; \mathbf{p}_0) f(\mathbf{p}_2; -\mathbf{p}_0) + f(\mathbf{p}_2; \mathbf{p}_0) f(\mathbf{p}_1; -\mathbf{p}_0)] \quad (6)$$

which can be rewritten as

$$\frac{d^2\Sigma}{d\Omega_1 d\Omega_2} = \frac{1}{2} \int d\Omega_0 \frac{d\sigma}{d\Omega_0} \int \frac{p_1^2 dp_1}{E_1} \frac{p_2^2 dp_2}{E_2} [f_F(p_{T1}) f_B(p_{T2}) + f_F(p_{T2}) f_B(p_{T1})] \quad (7)$$

After replacing  $p$  with  $p_T/\sin\eta$  ( $\eta$  is the scattering angle with respect to the original jet axis) in the forward hemisphere and  $p$  with  $p_T/\sin(\pi - \eta)$  in the backward hemisphere, we obtain

$$\frac{d^2\Sigma}{d\Omega_1 d\Omega_2} = \frac{1}{2} \int d\Omega_0 \frac{d\sigma}{d\Omega_0} [F(\eta_1) F(\pi - \eta_2) + F(\pi - \eta_1) F(\eta_2)] \quad (8)$$

where

$$F(\eta) = \frac{1}{E} \int p^2 dp f_F(p_T), \quad \text{for } \eta < \frac{\pi}{2} \quad (9)$$

From (3) we see that

$$\int d\Omega F(\eta) = 1. \quad (10)$$

Using relation  $p = p_T/\sin\eta$ , (9) can be written as

$$F(\eta) = \frac{1}{E \sin^3 \eta} \int_0^{E \sin \eta} p_T^2 dp_T f_F(p_T). \quad (11)$$

When  $\sin\eta \gg \langle p_T \rangle / E$ , we can use (5) and obtain

$$F(\eta) = \frac{\langle p_T \rangle}{2\pi E \sin^3 \eta}, \quad \text{for } \eta < \frac{\pi}{2} \quad (12)$$

Here  $\langle p_T \rangle$  is the average transverse momentum defined by

$$\langle p_T \rangle = \int p_T d^2 \mathbf{p}_T f(p_T). \quad (13)$$

The integration in (8) can be carried out numerically [6]. To obtain a simple analytical result, we note that in nuclear collisions only high transverse energy jets can be well identified. Also the study of jet propagation in longitudinal direction is very complicated by the fact that plasma expands in the same direction. For these reasons we restrict ourselves to the study of transverse jets. Near the transverse direction the  $d\sigma/d\Omega_0$  varies slowly with  $d\Omega_0$ , while  $F(\eta)$  varies rapidly near  $\eta = 0$ . Thus the dominating contributions to the integration in (8) come from small angular regions about the two detection directions  $\Omega_1$  and  $\Omega_2$ . As an example we consider the contribution from integration over the cone about  $\Omega_0 \approx \Omega_1$  which implies  $\eta_1 \approx 0$ ,  $\eta_2 \approx \phi$ . Here  $\phi$  is the angle between  $\Omega_1$  and  $\Omega_2$  on the transverse plane. Since the  $F(\eta_1)$  changes rapidly, we can expand  $d\sigma/d\Omega_0$  in the integrand as a Taylor series in  $\eta_1$  for fixed  $\phi$ . The dominating contribution to the integral over this region is then obtained by taking  $d\Omega_0 \approx d\Omega_1$ ,  $d\sigma/d\Omega_0 \approx d\sigma/\Omega_1$  and  $\eta_2 \approx \phi$ . The integral over  $\Delta\Omega_1$  becomes

$$\frac{d\sigma}{d\Omega_1} F(\pi - \phi) \int_{\Delta\Omega_1} d\Omega_1 F(\eta_1) = \frac{d\sigma}{d\Omega_1} F(\pi - \phi), \quad \text{for } \phi > \frac{\pi}{2} \quad (14)$$

Similarly, the integration over other cones can be evaluated. Summing over all contributions we obtain the double energy cross section

$$\frac{d^2\Sigma}{d\Omega_1 d\Omega_2} = \frac{1}{2} F(\pi - \phi) \left[ \frac{d\sigma}{d\Omega_1} + \frac{d\sigma}{d\Omega_2} \right], \quad \text{for } \phi > \frac{\pi}{2} \quad (15)$$

Integrating over double solid angle and keeping  $\phi$  constant we obtain the energy-energy correlation

$$\frac{1}{\Sigma} \frac{d\Sigma}{d\phi} = \frac{2\langle p_T \rangle}{\pi Q} \frac{1}{\sin^3(\pi - \phi)}, \quad \text{for } \phi > \frac{\pi}{2}, \quad (16)$$

and there is no correlation for  $\phi < \pi/2$  in the leading order approximation. Here  $Q$  is the total jet energy on the transverse plane. The asymmetry about  $\phi = \pi/2$  comes from the following fact. Because the  $f_F(p_T)$  and  $f_B(p_T)$  decrease rapidly with increase scattering angles with respect to two initial back-to-back jets, the correlation is the strongest at  $\phi = \pi$  and decreases monotonously with decreasing  $\phi$  and eventually vanishes at  $\phi = 0$ . The discontinuity of about  $\phi = \pi/2$  occurs because of the approximation. To

avoid the discontinuity we can extrapolate the correlation to the region  $\phi < \pi/2$  with

$$\frac{1}{\Sigma} \frac{d\Sigma}{d\phi} = \frac{2\langle p_T \rangle}{\pi Q} \sin \phi, \quad \text{for } \phi \leq \frac{\pi}{2}. \quad (17)$$

This is sensible because in  $\phi < \pi/2$  the correlation decreases monotonously to zero at  $\phi = 0$  as it should be, and the correlation function as well as its first derivative are continuous at  $\phi = \pi/2$ .

## 2.2 Multiple scattering in expanding plasmas

Now we turn to the calculation of  $\langle p_T \rangle$ . Let  $g(\mathbf{k}_T)$  be the normalized transverse momentum distribution of a jet after *one* scattering with a plasma constituent and  $P(n)$  be the normalized probability that a jet scattering  $n$  times with the constituents. The transverse momentum distribution of a jet after multiple scattering with plasma constituents is then

$$f(p_T) = \sum_{n=0} P(n) \int \prod_{i=1}^n d^2\mathbf{k}_{Ti} g(\mathbf{k}_{T1}) \cdots g(\mathbf{k}_{Tn}) \delta(\mathbf{p}_T - \sum_{j=1}^n \mathbf{k}_{Tj}), \quad (18)$$

with the understanding that  $f(\mathbf{p}_T) = \delta(\mathbf{p}_T)$  when  $n = 0$ . In an equilibrium plasma the multiple scatterings are independent from one another. In this case one can easily show

$$\langle p_T^2 \rangle = N \langle k_T^2 \rangle, \quad (19)$$

where  $\langle p_T^2 \rangle$  is the average transverse momentum after *multiple* scatterings defined as

$$\langle p_T^2 \rangle = \int d^2\mathbf{p}_T p_T^2 f_F(\mathbf{p}_T), \quad (20)$$

and  $\langle k_T^2 \rangle$  is the average transverse momentum after *one* scattering defined as

$$\langle k_T^2 \rangle = \int d^2\mathbf{k}_T k_T^2 g(\mathbf{k}_T), \quad (21)$$

and  $N$  is the average number of scatterings given by  $N = \sum_{n=0} nP(n)$ . Noting that the  $\langle p_T^2 \rangle$  is proportional to  $\langle p_T \rangle^2$ , and  $\langle k_T^2 \rangle$  to  $\langle k_T \rangle^2$ , and both distribution should be similar in shape, we expect

$$\langle p_T \rangle = \sqrt{N} \langle k_T \rangle, \quad (22)$$

In hydrodynamical models  $N$  can be calculated from

$$N = \int dx \left[ \sum_i n_i(x) \sigma_i \right]. \quad (23)$$

Here  $n_i$  is the particle density of the  $i$ th plasma constituent,  $\sigma_i$  is the scattering cross section of a jet with the  $i$ th constituent. The integral is carried out along the jet trajectory.

We consider central nuclear collisions where the created plasma is constrained in a cylinder of radius  $R = 1.2A^{1/3}$  (fm) where  $A$  is the nuclear mass number. The evolution of the plasma after its formation is described by hydrodynamical equations. In the Bjorken model [7] the system expands isentropically along the longitudinal direction and the entropy density decreases according to

$$s(\tau) = s(\tau_i) \tau_i / \tau \quad (24)$$

while the temperature falls according to

$$T(\tau) = T_i [\tau_i / \tau]^{1/3} \quad (25)$$

where  $\tau_i$  is the proper time at which the plasma is formed and  $T_i$  is its initial temperature. When the temperature drops to  $T_c$  at time  $\tau_c$  a mixed phase emerges. In the end of the mixed phase at time  $\tau_h$  the system is fully converted into hadrons. It can be shown that

$$\tau_h = r \tau_c \quad (26)$$

where  $r$  is the ratio of degree of freedoms in the plasma phase to that in the hadronic phase.

Now let us rewrite (23) as

$$N = \sigma_{pl} \int d\tau n(\tau) \quad (27)$$

where  $\sigma_{pl}$  is the averaged cross section and  $n(\tau)$  is the total particle density in plasma. In the additive quark model the quark-quark cross section is  $\sigma_{qq} \approx 4$  mb and in perturbative QCD one has  $\sigma_{gg} = (9/4)\sigma_{qq} = (9/4)^2\sigma_{qq}$ . Hence, we might expect  $\sigma_{pl} \approx (16 + 4.6N_f)/(16 + 12N_f)\sigma_{gg} \approx 12$  mb. Noting



that for an idea gas the particle density is proportional to the entropy density and using the expansion equation (24) we have

$$N = \sigma_{pl}\tau_i n(\tau_i) \ln(\tau_f/\tau_i) \quad (28)$$

where  $n(\tau_i)$  is the initial particle density.  $\tau_f$  is the time for the jets to escape from the plasma, if this happens before beginning of the mixed phase, i.e.  $\tau_f < \tau_c$ . When  $\tau_f > \tau_c$  jets will interact with the mixed phase constituents: quarks, gluons and hadrons.

Because of the large degree of freedom in the plasma phase (c.f. eq. 26), the mixed phase is long and jets propagating transversal to collision direction are expected to escape from the plasma before the completion of mixed phase. Thus hadronic gas has no effects on jets.

We note  $\sigma_{q\pi} = (2/9)\sigma_{pp} \approx 9$  mb. For simplicity we assume  $\sigma_{q\pi} = \sigma_{pl}$ . In this case the number of collisions can still be expressed by (28). There  $\tau_f$  is the escape time of jets which may have been scattered by mixed phase constituents. When a jet pair is created at a distance  $R_0$  from the collision axis, the average number of collisions each jet experienced is

$$N = \frac{1}{2}\sigma_{pl}\tau_i n(\tau_i) \ln \frac{R^2 - R_0^2}{\tau_i^2} \quad (29)$$

and  $N = 0$  if  $R^2 - R_0^2 \leq \tau_i^2$ . Since  $R_0$  is unmeasurable, an average over geometry must be made. For a sharp nuclear density profile we obtain

$$N = \frac{1}{2}\sigma_{pl}\tau_i n(\tau_i) \left[ \ln \frac{R^2}{\tau_i^2} - \frac{1}{2} + \frac{\tau_i^4}{2R^4} \right] \quad (30)$$

Noting that  $n(\tau_i) = s(\tau_i)/c$  with  $c = 3.6$ , we obtain

$$N = \frac{g_Q\pi^2}{45c}\sigma_{pl}\tau_i T_i^3 \left[ \ln \frac{R^2}{\tau_i^2} - \frac{1}{2} + \frac{\tau_i^4}{2R^4} \right] \quad (31)$$

where  $g_Q = 16 + 21N_f/2$  is the degree of freedom in plasma and  $N_f$  is the number of active quark flavor.

In the above calculations only longitudinal expansion is taken into account. When the system expands transversally as well, it will take longer for jets to escape from the plasma. This may increase the number of collision and enhance plasma effects. On the other hand, transverse expansion accelerates

the cooling process and reduces plasma density more rapidly. Hence, the resulting effects is expected to be small. Furthermore, we note that transverse expansion is negligible in the early stage of the expansion. As a result, the transverse expansion has little effects on jets.

### 2.3 Hadronization

The results obtained so far are for quarks and gluons. To compare with experiments, the effects of hadronization should be taken into account. Basham et al. [2] have calculated that the hadronization correction to the energy pattern and correlations. Similarly one can show that the hadronization correction to the transverse energy–energy correlations is given by

$$\frac{c_0 \langle h_T \rangle}{\pi Q \sin^3 \phi}, \quad \text{for } \phi < \pi. \quad (32)$$

Here  $c_0 = 2.5$  is the multiplicity density at rapidity  $y = 0$  and  $\langle h_T \rangle$  is the average transverse momentum of hadrons from jet fragmentation [2]. Because two hadrons with angle  $\phi$  may come from either the same jet or from the two separate back-to-back jets, the hadronization correction to correlation is symmetric about  $\phi = \pi/2$ .

Summing over the effects of QCD corrections, multiple scattering in plasma and hadronization, we finally obtain the energy–energy correlation

$$\frac{1}{\Sigma} \frac{d\Sigma}{d\phi} = \frac{1}{\Sigma} \frac{d\Sigma^{(QCD)}}{d\phi} + \begin{cases} \frac{2\sqrt{N} \langle k_T \rangle + c_0 \langle h_T \rangle}{\pi Q \sin^3(\pi - \phi)} & \text{for } \phi > \pi/2 \\ \frac{2\sqrt{N} \langle k_T \rangle \sin \phi}{\pi Q} + \frac{c_0 \langle h_T \rangle}{\pi Q \sin^3 \phi} & \text{for } \phi \leq \pi/2. \end{cases} \quad (33)$$

## 3 Results and discussion

From (33) and (31) we see that the results depend on three parameters, the initial temperature  $T_i$ , the jet energy  $Q$  and the geometrical size  $R$ , that can be changed in experiments.

We first look at central Au–Au collisions at RHIC energy (200 GeV per nucleon) where the initial temperature is expected to be about 250 MeV. The results for correlations are shown in Figs. 1 at jet energies  $Q = 10$ , and 20

GeV. In the calculation we used  $N_f = 3$ ,  $\sigma_{pl} = 12$  mb,  $\Lambda = 0.2$  GeV,  $\tau_i = 1$  fm,  $\langle k_T \rangle = \langle h_T \rangle = 0.36$  GeV and the results of refs. [4, 5] for  $d\Sigma^{(QCD)}/d\phi$ . As we can see from the figure that the hadronization effects are unimportant at  $Q = 20$  GeV, while the plasma effects are distinctly beyond the QCD effects. To minimized the hadronization effects one studies the asymmetric correlations defined as [2]

$$A(\phi) = \frac{1}{\Sigma} \left[ \frac{d\Sigma}{d\phi}(\pi - \phi) - \frac{d\Sigma}{d\phi}(\phi) \right], \quad \text{for } \phi < \pi/2 \quad (34)$$

In Fig. 2 we show the corresponding  $A(\phi)$  distributions. From the figure we see that the plasma effects are significant and should be easily measured experimentally if the plasma is created in the collision. Here the hadronization effects cancel because of the symmetry about  $\phi = \pi/2$ .

In Figs. 3 and 4 we show the  $(1/\Sigma)(d\Sigma/d\phi)$  and  $A(\phi)$ , respectively, for  $Q = 40$ , and 100 GeV at LHC energy (6300 GeV per nucleon) where we estimate  $T_i = 500$  MeV. Compare Fig. 1 with 3 and 2 with 4 we see that plasma effects increase with increasing initial temperature. At LHC the plasma effects stand well beyond the effects of QCD corrections and hadronizations for jet energy as high as 100 GeV.

To see the plasma effects more directly, one might compare the integrations that are defined as

$$\sigma_C = \int_{\phi_1}^{\phi_2} \frac{1}{\Sigma} \frac{d\Sigma}{d\phi}(\phi) d\phi \quad (35)$$

for energy–energy correlations and,

$$\sigma_A = \int_{\phi_1}^{\phi_2} A(\phi) d\phi \quad (36)$$

for asymmetric energy–energy correlations. The results for various  $T_i$  and  $Q$  are listed in Tables 1 and 2 respectively. Here we integrated over  $\phi$  from  $\pi/6$  to  $5\pi/6$  for  $\sigma_C$ , and from  $\pi/6$  to  $\pi/2$  for  $\sigma_A$ . From the tables we see that the integrations are enhanced by a factor of 1.2 to 1.6 due to the presence of the plasma. In  $e^+e^-$  experiments the integration can be very well determined [8]. Similarly, we expect that such enhancement can be unambiguously measured in high  $Q$  jet events in heavy ion collisions.

Table 1: Integrations of energy–energy correlation function for various  $T_i$  and  $Q$

$T_i$ (MeV)	$Q$ (GeV)	QCD	QCD+Hadr.	QCD+Hadr.+Plasma
250	10	1.29	1.54	2.27
250	20	1.32	1.44	1.80
500	40	0.93	0.99	1.51
500	100	0.95	0.98	1.19

Table 2: Integrations of asymmetric energy–energy correlation function for various  $T_i$  and  $Q$

$T_i$ (MeV)	$Q$ (GeV)	QCD	QCD+Hadr.	QCD+Hadr.+Plasma
250	10	0.76	0.76	1.12
250	20	0.33	0.33	0.52
500	40	0.54	0.54	0.80
500	100	0.24	0.24	0.35

In central collisions the initial particle density increases with  $A^{1/3}$ . When  $R \gg \tau_i$  the number of scatterings increases with  $A^{1/3} \ln(R^2/\tau_i^2)$ . In Figs. 5 and 6 the  $(1/\Sigma)(d\Sigma/d\phi)$  and  $A(\phi)$  distributions for  $Q = 40$  GeV for S–S collision are compared with those for Au–Au collision at LHC, respectively. We see that the results depend rather weakly on the nuclear geometry.

We note that in the kinematic region that we are interested in, dominating effects are from scatterings of two gluon jets, and our results are not applicable to scattering angle  $\sin \eta_{\lesssim} \langle p_T \rangle / Q$  which corresponds to the region of  $\phi \approx 0$  and  $\phi \approx \pi$ .

In small scattering angle the multiple soft gluon bremsstrahlung plays an important role [9,10]. In the regions of  $\phi \approx 0$  and  $\phi \approx \pi$  one might study the momentum imbalance or acoplanarity as suggested by Appel [9], Blaizot and McLerran [10].

## 4 Conclusions

We used (asymmetric) transverse energy–energy correlations to study the effects of multiple scatterings of jets on constituents of quark gluon plasma. In the calculations we considered the expansion of plasma, QCD corrections and nonperturbative effects. Our results show that the scattering effects are remarkably strong in (asymmetric) correlations. At LHC they stand well above the background from QCD corrections and hadronizations for jet energy as high as 100 GeV. If the plasma is formed in nuclear collisions and go through a phase transition, the jets are expected to escape before the completion of mixed phase due to the large degree of freedom in plasma. In this case the observed effects are free of final state hadronic interactions and decays. These imply that jets could be used to probe the quark gluon plasma.

The plasma effects increases with decreasing jet energy. To obtain maximal effects, jet energy should be kept as low as possible. We note, however, that low energy jets, or minijets, can be created or quenched due to multiple interactions with plasma constituents. Because of fluctuation in soft processes [11], it is also elusive to identify minijets in experiments. To avoid such backgrounds and experimental ambiguities, jet energy should be kept high enough. Total jet energies of  $Q = 10$  and 40 GeV might be sensible thresholds at RHIC and LHC energies, respectively.

The main background of jet signature is probably the hadronic gas. When jets propagate in hadronic gas, the multiple scattering between jets and hadrons results in similar effects as plasmas do. In general one expects that hadronic gas exists at lower temperature. In very high energy heavy ion collisions, such as RHIC and LHC, the effects from hadronic gas should be smaller than those from plasmas. To make quantitative comparison, realistic models and detailed calculations are necessary [6].

## Acknowledgments

We would like to thank H.C. Eggers for useful discussions. This work was supported in part by the National Sciences and Engineering Research Council of Canada, and in part by the FCAR fund of the Québec Government.

## References

- [1] See, e.g., Advanced Series on Directions in High Energy Physics, *Quark Gluon Plasma*, edited by R. C. Hwa, (World Scientific, 1990); proceedings of *Quark Matter '91*, Gatlinburg, Tennessee, USA, 1991, edited by T.C. Awes, et al. (North-Holland, 1992); proceedings of *Quark Matter '93*, Borlänge, Sweden, 1993, (to be published); and references therein.
- [2] C.L. Basham, L.S. Brown, S.D. Ellis and S.T. Love, Phys. Rev. **D17**, 2298 (1978), Phys. Rev. Lett. **41**, 1585 (1978), Phys. Rev. **D19**, 2018 (1979), Phys. Rev. **D24**, 2382 (1981).
- [3] See for examples: P. Abreu et al. (DELPHI Coll.), Phys. Lett. **B252** , 149 (1990), M.Z.Akrawy et al. (OPAL Coll.), Phys. Lett. **B252** , 159 (1990), B.Adeva et al. (L3 Coll.), Phys. Lett. **B257**, 469 (1991), and references cited therein.
- [4] A. Ali, E. Pietarinen and W.J. Stirling, Phys. Lett. **B141**, 447 (1984).
- [5] J. Kripfganz and A. Schiller, Phys. Lett. **B79**, 317 (1978); A. Schiller, J. Phys. **G5**, 1329 (1979); T. Gottschalk and D. Sivers, Phys. Rev. **D21**, 102 (1980); F.A. Berends et al. Phys. Lett. **B103**, 124 (1981); Z. Kunszt and E. Pietarinen, Nucl. Phys. **B164**, 45 (1980); Phys. Lett. **B132**, 453 (1983).
- [6] Jicai Pan and Charles Gale, in preparation.
- [7] J.D. Bjorken, Phys. Rev. **D27**, 140 (1983).
- [8] D. Schlatter et al., Phys. Rev. Lett **49**, 521 (1982), and [2,3]
- [9] D.A. Appel, Phys. Rev. **D33**, 717 (1986).
- [10] J.P. Blaizot and L. McLerran , Phys. Rev. **D34**, 2739 (1986).
- [11] W.Q. Chao, T. Meng and J. Pan , Phys. Rev. Lett. **58**, 1399 (1987); T. Meng and J. Pan , Phys. Rev. **D37**, 243 (1988).

## Figure captions

**Fig. 1** The  $(1/\Sigma)(d\Sigma/d\phi)$  distribution for  $T_i = 250$  MeV in Au–Au collisions. (a) for total transverse jet energy  $Q = 10$  GeV, and (b) for  $Q = 20$  GeV.

**Fig. 2** The  $A(\phi)$  distribution for the same parameters as those in Fig. 1. (a) for  $Q = 10$  GeV, and (b) for  $Q = 20$  GeV.

**Fig. 3** The  $(1/\Sigma)(d\Sigma/d\phi)$  distribution for  $T_i = 500$  MeV in Au–Au collisions. (a) for  $Q = 40$  GeV, and (b) for  $Q = 100$  GeV.

**Fig. 4** The  $A(\phi)$  distribution for the same parameters as those in in Fig. 3. (a) for  $Q = 20$  GeV, and (b) for  $Q = 100$  GeV.

**Fig. 5** The comparison of  $(1/\Sigma)(d\Sigma/d\phi)$  distribution for S–S and Au–Au collisions for  $Q = 40$  GeV at  $T_i = 500$  MeV in Au–Au collisions.

**Fig. 6** The comparison of  $A(\phi)$  distribution for S–S and Au–Au collisions for the same parameters as those in Fig. 5.

This figure "fig1-1.png" is available in "png" format from:

<http://arxiv.org/ps/hep-ph/9406208v1>



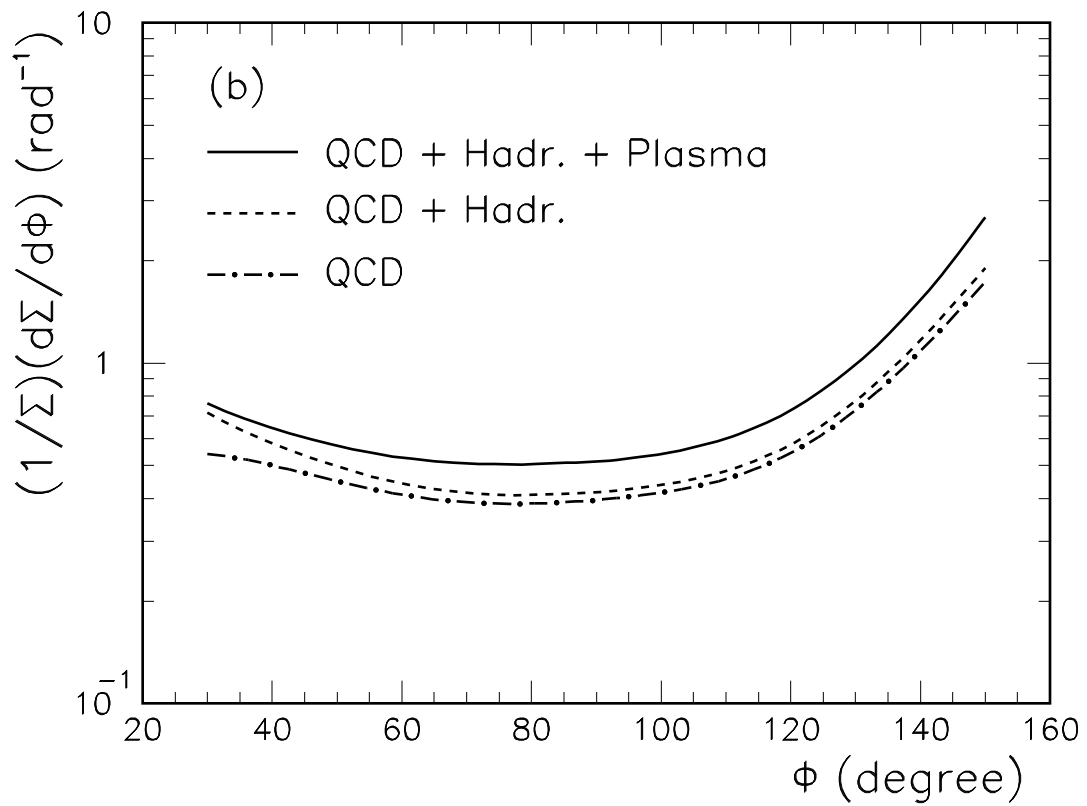
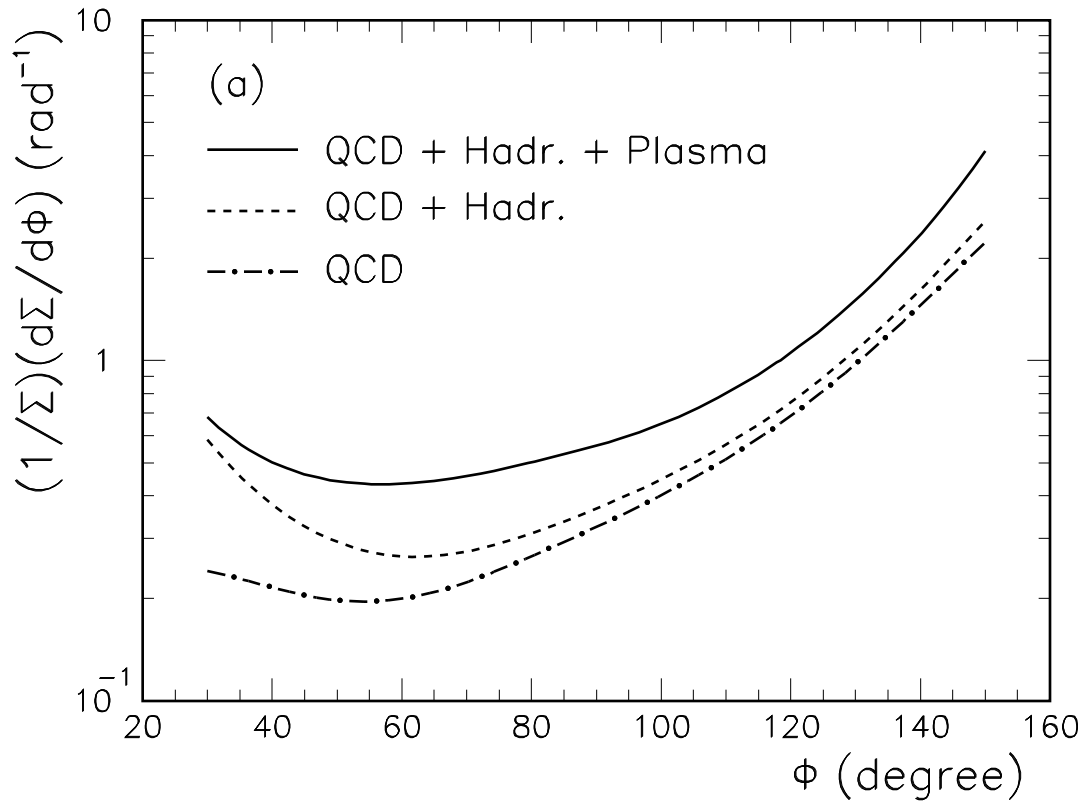


Fig. 1

This figure "fig1-2.png" is available in "png" format from:

<http://arxiv.org/ps/hep-ph/9406208v1>

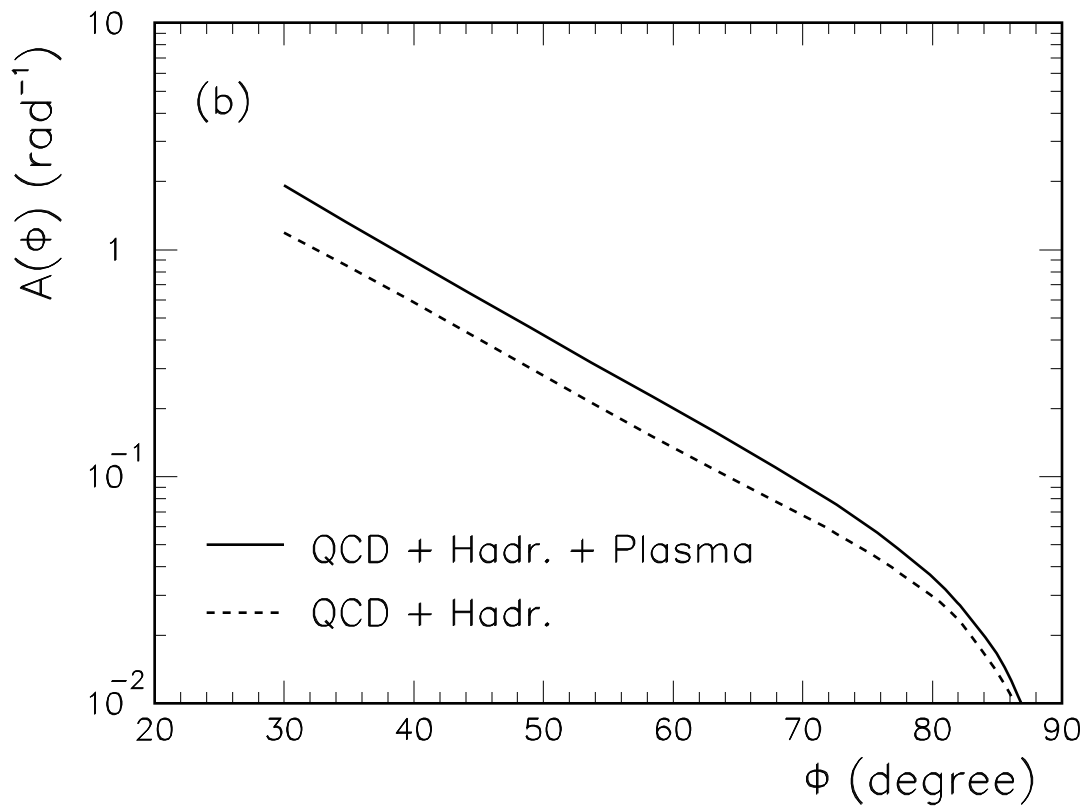
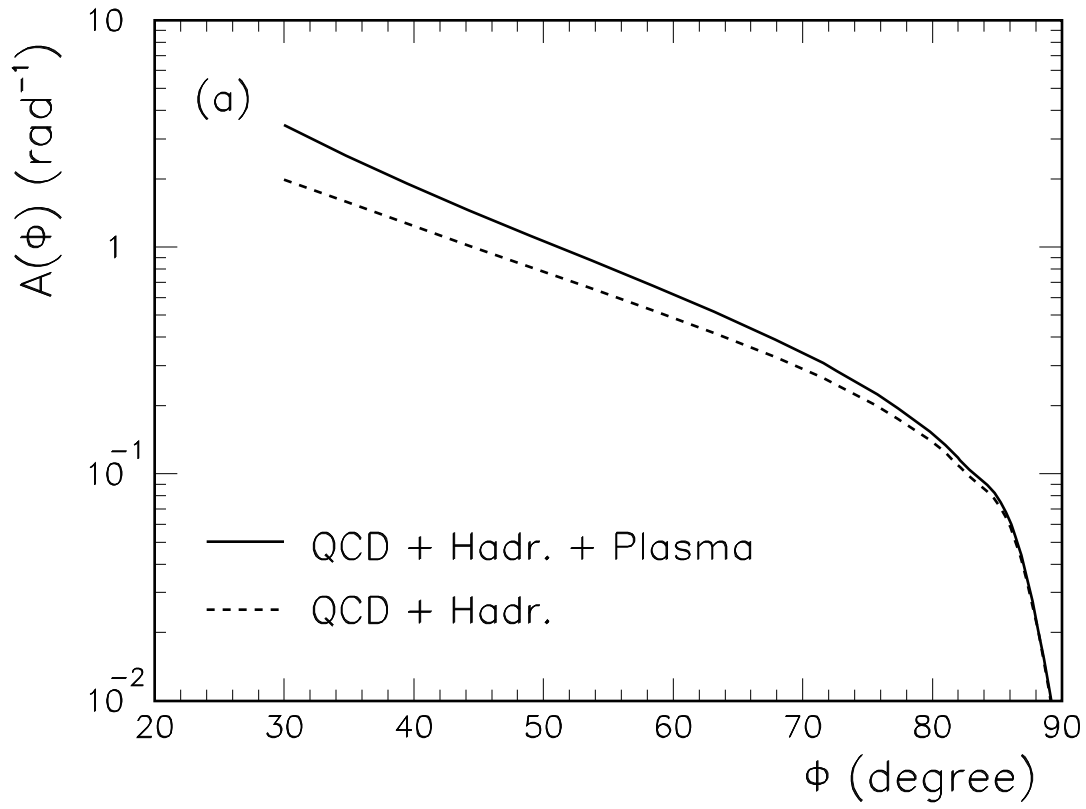


Fig. 2

This figure "fig1-3.png" is available in "png" format from:

<http://arxiv.org/ps/hep-ph/9406208v1>

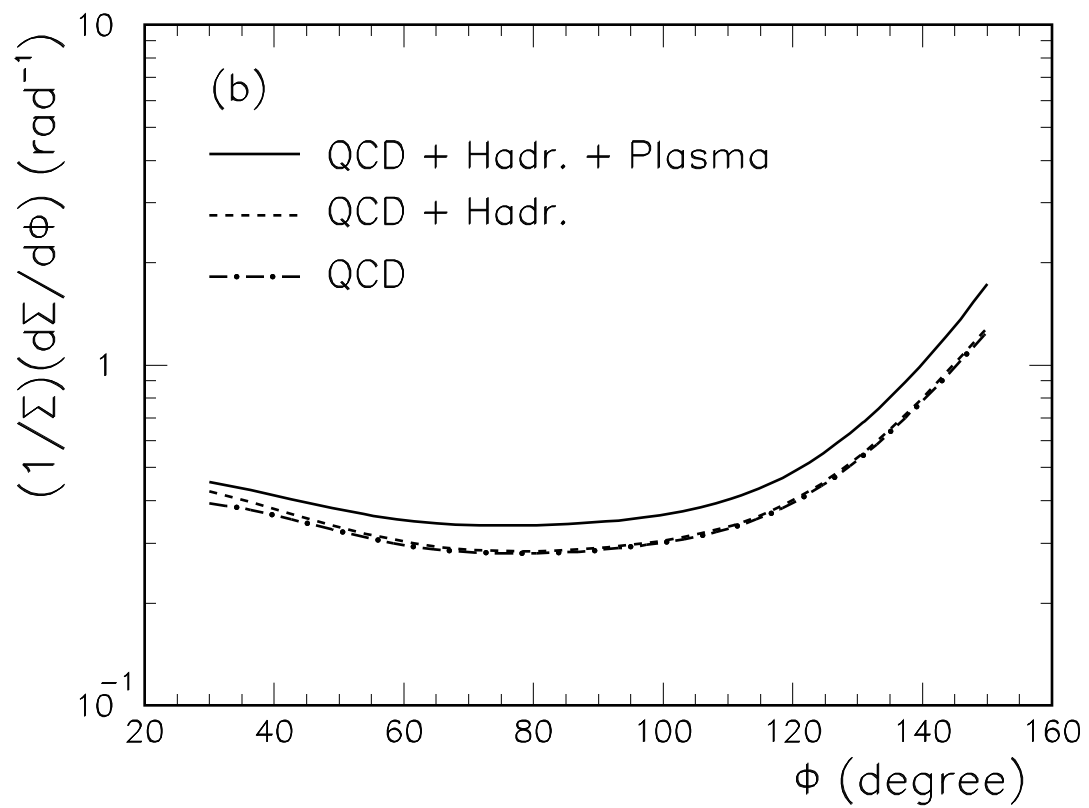
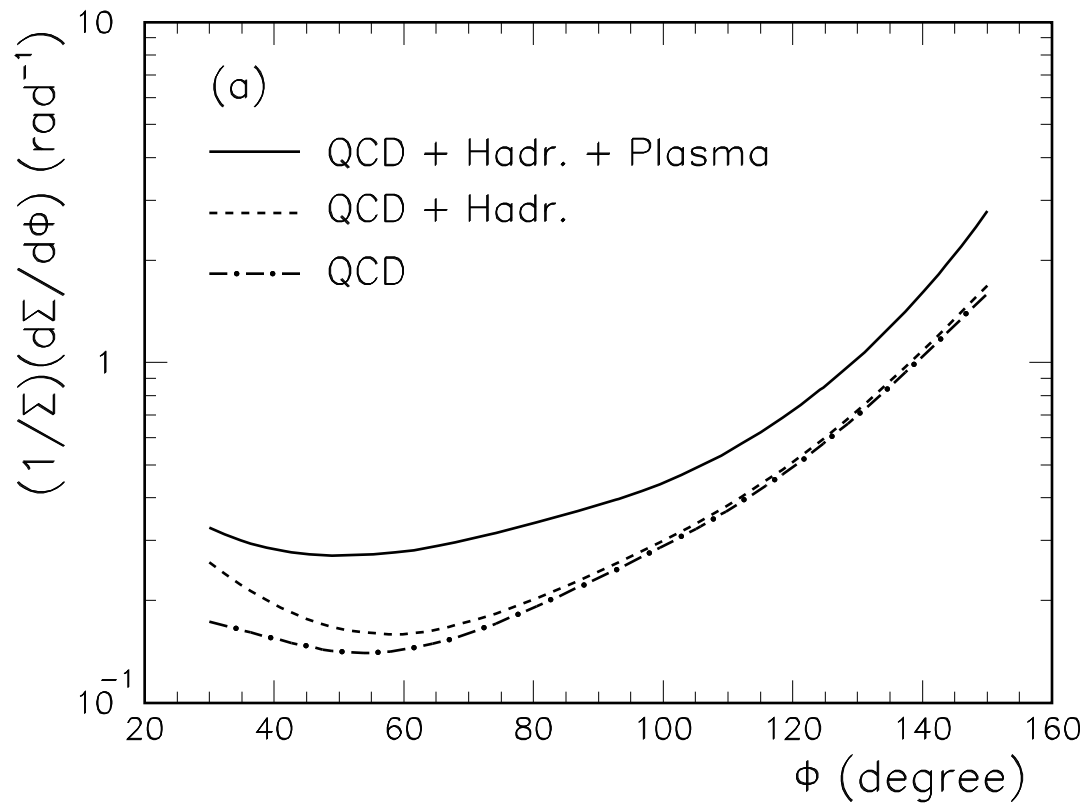


Fig. 3

This figure "fig1-4.png" is available in "png" format from:

<http://arxiv.org/ps/hep-ph/9406208v1>

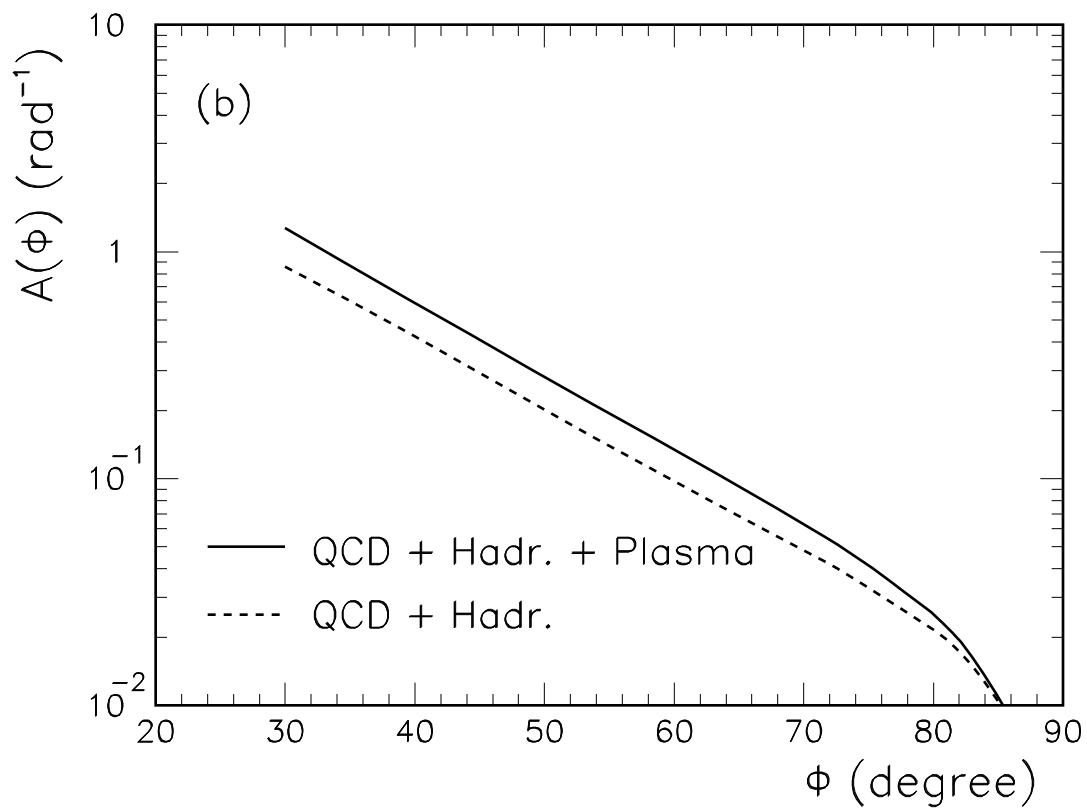
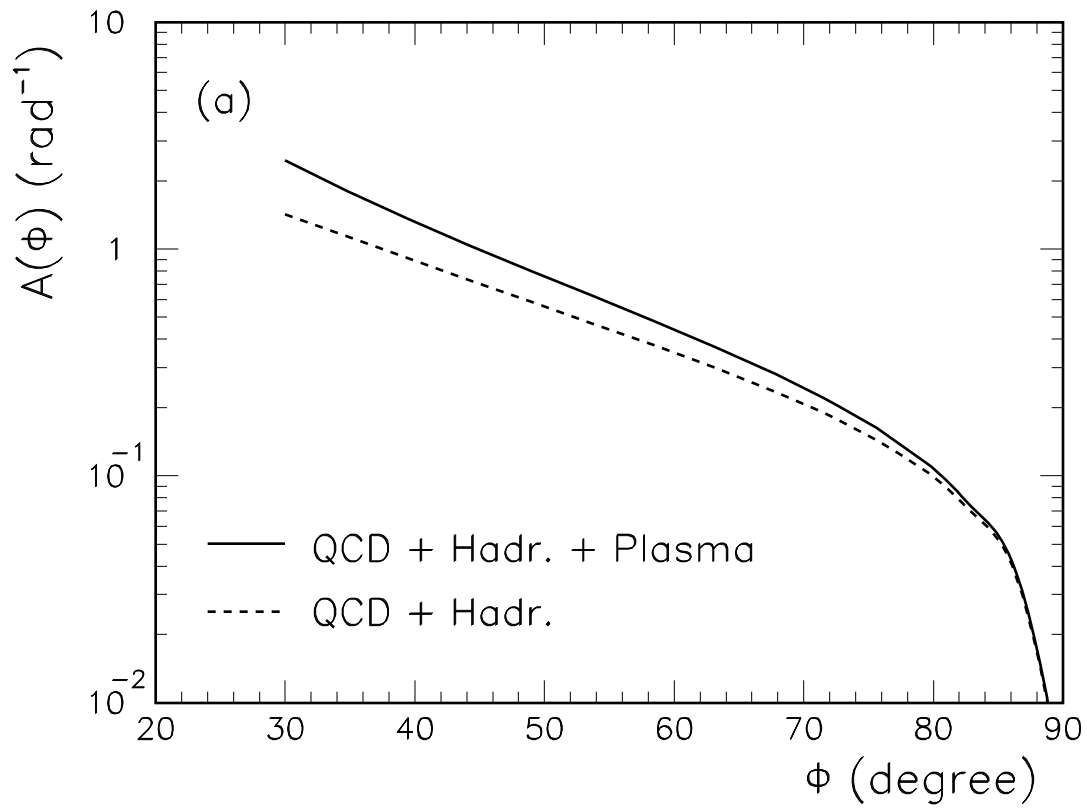


Fig. 4

This figure "fig1-5.png" is available in "png" format from:

<http://arxiv.org/ps/hep-ph/9406208v1>



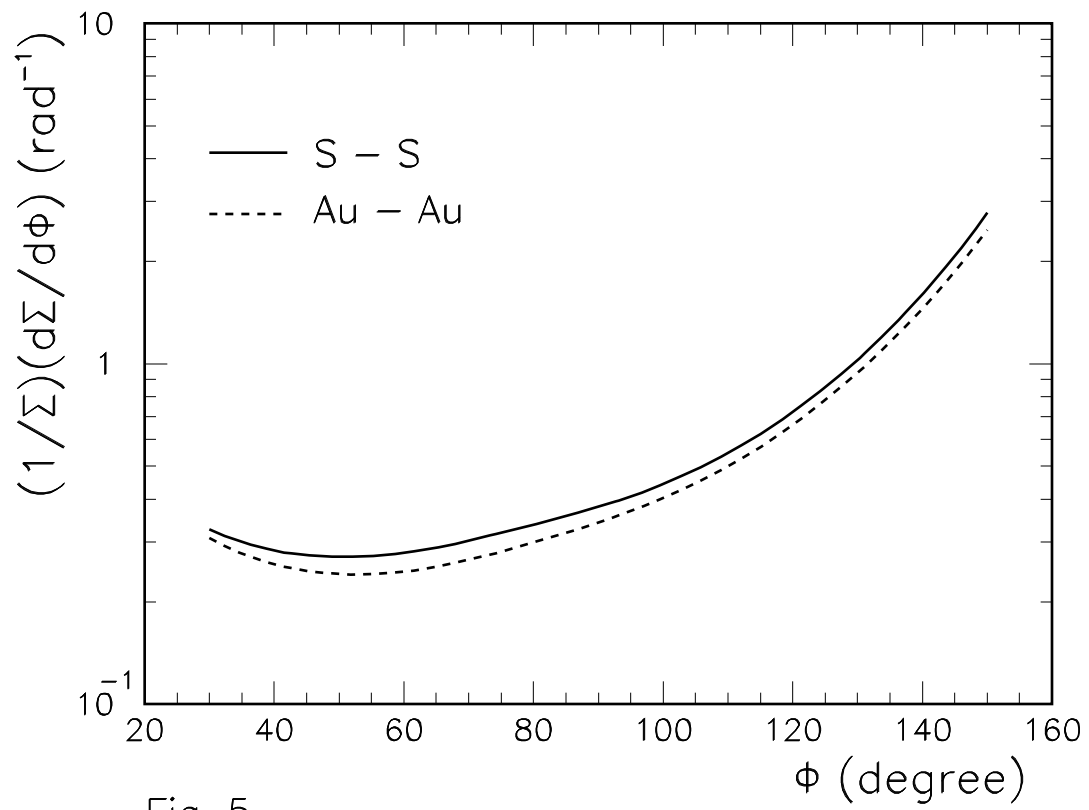


Fig. 5

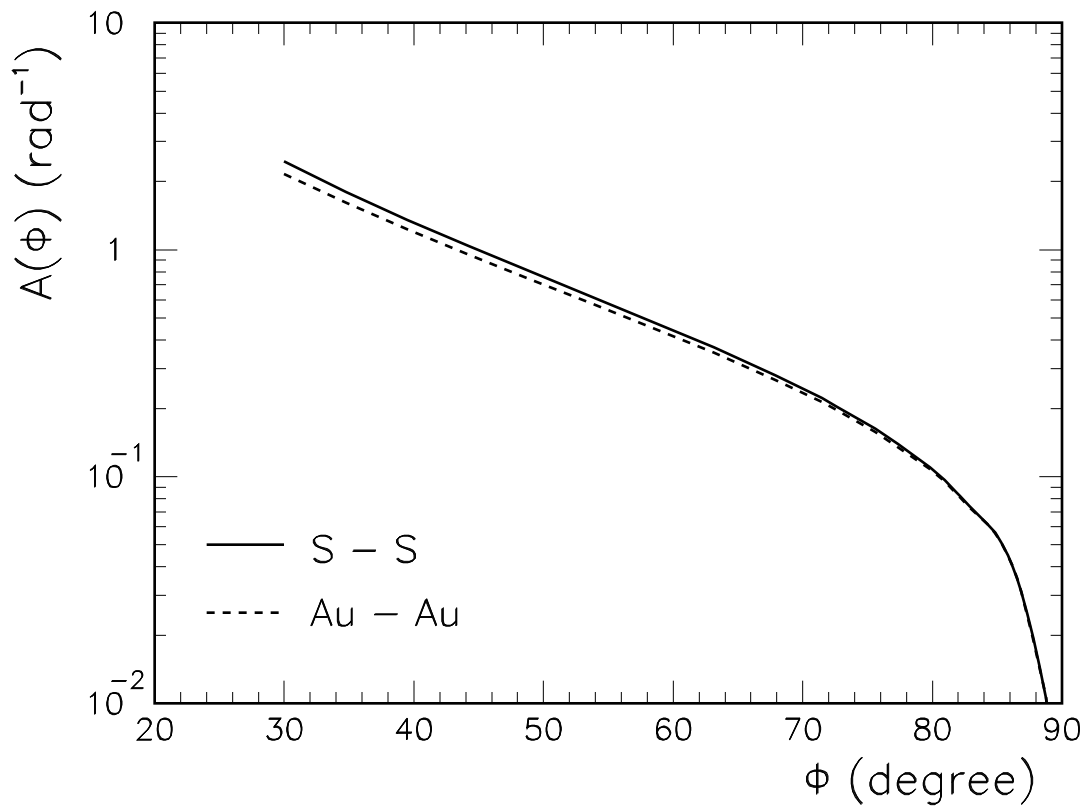


Fig. 6